Research Article | Vol. 25, No. 18 | 4 Sep 2017 | OPTICS EXPRESS 21753
Optics EXPRESS

Two-dimensional coherent spectroscopy of a THz quantum cascade laser: observation of multiple harmonics

SERGEJ MARKMANN,[1,4,6] HANOND NONG,[1] SHOVON PAL,[2,5] TOBIAS FOBBE,[1,2] NEGAR HEKMAT,[1] RESHMA A. MOHANDAS,[3] PAUL DEAN,[3] LIANHE LI,[3] EDMUND H. LINFIELD,[3] A. GILES DAVIES,[3] ANDREAS D. WIECK,[2] AND NATHAN JUKAM,[1,7]

[1]*AG Terahertz Spektroskopie und Technologie, Ruhr-Universität Bochum, D-44780 Bochum, Germany*
[2]*Lehrstuhl für Angewandte Festkörperphysik, Ruhr-Universität Bochum, D-44780 Bochum, Germany*
[3]*School of Electronic and Electrical Engineering, University of Leeds, Leeds LS2 9JT, UK*
[4]*Current address: IBM Research-Zurich, 8803 Rüschlikon, Switzerland*
[5]*Current address: Department of Materials, ETH Zürich, 8093 Zürich, Switzerland*
[6]*sergej.markmann@rub.de*
[7]*nathan.jukam@rub.de*

Abstract: Two-dimensional spectroscopy is performed on a terahertz (THz) frequency quantum cascade laser (QCL) with two broadband THz pulses. Gain switching is used to amplify the first THz pulse and the second THz pulse is used to probe the system. Fourier transforms are taken with respect to the delay time between the two THz pulses and the sampling time of the THz probe pulse. The two-dimensional spectrum consists of three peaks at ($\omega_\tau = 0$, $\omega_t = \omega_0$), ($\omega_\tau = \omega_0$, $\omega_t = \omega_0$), and ($\omega_\tau = 2\omega_0$, $\omega_t = \omega_0$) where ω_0 denotes the lasing frequency. The peak at $\omega_\tau = 0$ represents the response of the probe to the zero-frequency (rectified) component of the instantaneous intensity and can be used to measure the gain recovery.

OCIS codes: (300.6240) Spectroscopy, coherent transient; (140.5965) Semiconductor lasers, quantum cascade; (300.6495) Spectroscopy, terahertz; (140.3070) Infrared and far-infrared lasers.

References and links

1. D. M. Jonas, "Two-dimensional femtosecond spectroscopy," Annu. Rev. Phys. Chem. **54**(1), 425–463 (2003).
2. A. M. Brańczyk, D. B. Turner, and G. D. Scholes, "Crossing disciplines - A view on two-dimensional optical spectroscopy," Ann. Phys. **526**(1-2), 31–49 (2014).
3. K. W. Stone, K. Gundogdu, D. B. Turner, X. Li, S. T. Cundiff, and K. A. Nelson, "Two-quantum 2D FT electronic spectroscopy of biexcitons in GaAs quantum wells," Science **324**(5931), 1169–1173 (2009).
4. X. Li, T. Zhang, C. N. Borca, and S. T. Cundiff, "Many-body interactions in semiconductors probed by optical two-dimensional fourier transform spectroscopy," Phys. Rev. Lett. **96**(5), 057406 (2006).
5. W. Kuehn, K. Reimann, M. Woerner, T. Elsaesser, R. Hey, and U. Schade, "Strong correlation of electronic and lattice excitations in GaAs/AlGaAs semiconductor quantum wells revealed by two-dimensional terahertz spectroscopy," Phys. Rev. Lett. **107**(6), 067401 (2011).
6. T. Maag, A. Bayer, S. Baierl, M. Hohenleutner, T. Korn, C. Schüller, D. Schuh, D. Bougeard, C. Lange, R. Huber, M. Mootz, J. E. Sipe, S. W. Koch, and M. Kira, "Coherent cyclotron motion beyond Kohn's theorem," Nat. Phys. **12**(2), 119–123 (2015).
7. J. Lu, X. Li, H. Y. Hwang, B. K. Ofori-Okai, T. Kurihara, T. Suemoto, and K. A. Nelson, "Coherent Two-Dimensional Terahertz Magnetic Resonance Spectroscopy of Collective Spin Waves," Phys. Rev. Lett. **118**(20), 207204 (2017).
8. P. Hamm and M. Zanni, *Concepts and Methods of 2D Infrared Spectroscopy* (Cambridge University, 2011).
9. J. Zheng, K. Kwak, and M. D. Fayer, "Ultrafast 2D IR vibrational echo spectroscopy," Acc. Chem. Res. **40**(1), 75–83 (2007).
10. J. Zheng, K. Kwak, J. Asbury, X. Chen, I. R. Piletic, and M. D. Fayer, "Ultrafast dynamics of solute-solvent complexation observed at thermal equilibrium in real time," Science **309**(5739), 1338–1343 (2005).
11. S. Barbieri, W. Maineult, S. S. Dhillon, C. Sirtori, J. Alton, N. Breuil, H. E. Beere, and D. A. Ritchie, "13 GHz direct modulation of terahertz quantum cascade lasers," Appl. Phys. Lett. **91**(14), 143510 (2007).
12. C. Y. Wang, L. Kuznetsova, V. M. Gkortsas, L. Diehl, F. X. Kärtner, M. A. Belkin, A. Belyanin, X. Li, D. Ham,

#301501 https://doi.org/10.1364/OE.25.021753
Journal © 2017 Received 7 Jul 2017; revised 13 Aug 2017; accepted 14 Aug 2017; published 29 Aug 2017

Optics EXPRESS

H. Schneider, P. Grant, C. Y. Song, S. Haffouz, Z. R. Wasilewski, H. C. Liu, and F. Capasso, "Mode-locked pulses from mid-infrared quantum cascade lasers," Opt. Express **17**(15), 12929–12943 (2009).
13. S. Barbieri, M. Ravaro, P. Gellie, G. Santarelli, C. Manquest, C. Sirtori, S. P. Khanna, E. H. Linfield, and A. G. Davies, "Coherent sampling of active mode-locked terahertz quantum cascade lasers and frequency synthesis," Nat. Photonics **5**(5), 306–313 (2011).
14. J. R. Freeman, J. Maysonnave, N. Jukam, P. Cavalié, K. Maussang, H. E. Beere, D. A. Ritchie, J. Mangeney, S. S. Dhillon, and J. Tignon, "Direct intensity sampling of a modelocked terahertz quantum cascade laser," Appl. Phys. Lett. **101**(18), 181115 (2012).
15. F. Wang, K. Maussang, S. Moumdji, R. Colombelli, J. R. Freeman, I. Kundu, L. Li, E. H. Linfield, A. G. Davies, J. Mangeney, J. Tignon, and S. S. Dhillon, "Generating ultrafast pulses of light from quantum cascade Lasers," Optica **2**(11), 944 (2015).
16. D. Bachmann, M. Rösch, M. J. Süess, M. Beck, K. Unterrainer, J. Darmo, J. Faist, and G. Scalari, "Short pulse generation and mode control of broadband terahertz quantum cascade lasers," Optica **3**(10), 1087 (2016).
17. H. Choi, L. Diehl, Z.-K. Wu, M. Giovannini, J. Faist, F. Capasso, and T. B. Norris, "Gain Recovery Dynamics and Photon-Driven Transport in Quantum Cascade Lasers," Phys. Rev. Lett. **100**(16), 167401 (2008).
18. S. Liu, E. Lalanne, P. Q. Liu, X. Wang, C. F. Gmachl, and A. M. Johnson, "Femtosecond Carrier Dynamics and Nonlinear Effects in Quantum Cascade Lasers," IEEE J. Sel. Top. Quant. **18**(1), 92–104 (2012).
19. R. P. Green, A. Tredicucci, N. Q. Vinh, B. Murdin, C. Pidgeon, H. E. Beere, and D. A. Ritchie, "Gain recovery dynamics of a terahertz quantum cascade laser," Phys. Rev. B **80**(7), 075303 (2009).
20. D. R. Bacon, J. R. Freeman, R. A. Mohandas, L. Li, E. H. Linfield, A. G. Davies, and P. Dean, "Gain recovery time in a terahertz quantum cascade laser," Appl. Phys. Lett. **108**(8), 081104 (2016).
21. F. Eickemeyer, K. Reimann, M. Woerner, T. Elsaesser, S. Barbieri, C. Sirtori, G. Strasser, T. Müller, R. Bratschitsch, and K. Unterrainer, "Ultrafast coherent electron transport in semiconductor quantum cascade structures," Phys. Rev. Lett. **89**(4), 047402 (2002).
22. W. Kuehn, W. Parz, P. Gaal, K. Reimann, M. Woerner, T. Elsaesser, T. Müller, J. Darmo, K. Unterrainer, M. Austerer, G. Strasser, L. R. Wilson, J. W. Cockburn, A. B. Krysa, and J. S. Roberts, "Ultrafast phase-resolved pump-probe measurements on a quantum cascade laser," Appl. Phys. Lett. **93**(15), 151106 (2008).
23. C. Worrall, J. Alton, M. Houghton, S. Barbieri, H. E. Beere, D. Ritchie, and C. Sirtori, "Continuous wave operation of a superlattice quantum cascade laser emitting at 2 THz," Opt. Express **14**(1), 171–181 (2006).
24. R. Köhler, A. Tredicucci, F. Beltram, H. E. Beere, E. H. Linfield, A. G. Davies, D. A. Ritchie, R. C. Iotti, and F. Rossi, "Terahertz semiconductor-heterostructure laser," Nature **417**(6885), 156–159 (2002).
25. S. Markmann, H. Nong, S. Pal, N. Hekmat, S. Scholz, N. Kukharchyk, A. Ludwig, S. Dhillon, J. Tignon, X. Marcadet, C. Bock, U. Kunze, A. D. Wieck, and N. Jukam, "Spectral modification of the laser emission of a terahertz quantum cascade laser induced by broad-band double pulse injection seeding," Appl. Phys. Lett. **107**(11), 111103 (2015).
26. G. C. Loata, M. D. Thomson, T. Löffler, and H. G. Roskos, "Radiation field screening in photoconductive antennae studied via pulsed terahertz emission spectroscopy," Appl. Phys. Lett. **91**(23), 232506 (2007).
27. H. Nong, S. Pal, S. Markmann, N. Hekmat, R. A. Mohandas, P. Dean, L. Li, E. H. Linfield, A. G. Davies, A. D. Wieck, and N. Jukam, "Narrow-band injection seeding of a terahertz frequency quantum cascade laser: Selection and suppression of longitudinal modes," Appl. Phys. Lett. **105**(11), 111113 (2014).
28. G. Zhao, R. N. Schouten, N. van der Valk, W. Th. Wenckebach, and P. C. M. Planken, "Design and performance of a THz emission and detection setup based on a semi-insulating GaAs emitter," Rev. Sci. Instrum. **73**(4), 1715–1719 (2002).
29. D. Oustinov, N. Jukam, R. Rungsawang, J. Madéo, S. Barbieri, P. Filloux, C. Sirtori, X. Marcadet, J. Tignon, and S. Dhillon, "Phase seeding of a terahertz quantum cascade laser," Nat. Commun. **1**(6), 69 (2010).
30. D. Bachmann, N. Leder, M. Rösch, G. Scalari, M. Beck, H. Arthaber, J. Faist, K. Unterrainer, and J. Darmo, "Broadband terahertz amplification in a heterogeneous quantum cascade laser," Opt. Express **23**(3), 3117–3125 (2015).
31. J. Kröll, J. Darmo, S. S. Dhillon, X. Marcadet, M. Calligaro, C. Sirtori, and K. Unterrainer, "Phase-resolved measurements of stimulated emission in a laser," Nature **449**(7163), 698–701 (2007).
32. N. Jukam, S. S. Dhillon, D. Oustinov, J. Madéo, J. Tignon, R. Colombelli, P. Dean, M. Salih, S. P. Khanna, E. H. Linfield, and A. G. Davies, "Terahertz time domain spectroscopy of phonon-depopulation based quantum cascade lasers," Appl. Phys. Lett. **94**(25), 251108 (2009).
33. N. Jukam, S. S. Dhillon, D. Oustinov, Z.-Y. Zhao, S. Hameau, J. Tignon, S. Barbieri, A. Vasanelli, P. Filloux, C. Sirtori, and X. Marcadet, "Investigation of spectral gain narrowing in quantum cascade lasers using terahertz time domain spectroscopy," Appl. Phys. Lett. **93**(10), 101115 (2008).
34. N. Jukam, S. S. Dhillon, D. Oustinov, J. Julien Madeo, C. Manquest, S. Barbieri, C. Sirtori, S. P. Khanna, E. H. Linfield, A. G. Davies, and J. Tignon, "Terahertz amplifier based on gain switching in a quantum cascade Laser," Nat. Photonics **3**(12), 715–719 (2009).
35. The THz pulses are modulated by placing an optical chopper in one arm of the Michelson interferometer.
36. J. Kim, V. M. Huxter, C. Curutchet, and G. D. Scholes, "Measurement of electron-electron interactions and correlations using two-dimensional electronic double-quantum coherence spectroscopy," J. Phys. Chem. A **113**(44), 12122–12133 (2009).
37. J. Kim, S. Mukamel, and G. D. Scholes, "Two-dimensional electronic double-quantum coherence spectroscopy," Acc. Chem. Res. **42**(9), 1375–1384 (2009).

Optics EXPRESS

38. D. B. Turner and K. A. Nelson, "Coherent measurements of high-order electronic correlations in quantum wells," Nature **466**(7310), 1089–1092 (2010).
39. J. Kröll, J. Darmo, K. Unterrainer, S. S. Dhillon, C. Sirtori, X. Marcadet, and M. Calligaro, "Longitudinal spatial hole burning in terahertz quantum cascade lasers," Appl. Phys. Lett. **91**(16), 161108 (2007).
40. J. Maysonnave, N. Jukam, M. S. M. Ibrahim, R. Rungsawang, K. Maussang, J. Madéo, P. Cavalié, P. Dean, S. P. Khanna, D. P. Steenson, E. H. Linfield, A. G. Davies, S. S. Dhillon, and J. Tignon, "Measuring the sampling coherence of a terahertz quantum cascade laser," Opt. Express **20**(15), 16662 (2012).

1. Introduction

Two-dimensional spectroscopy can be used to study the coherent coupling between molecular levels [1,2]. In solid-state physics, it has been applied to the study of excitons in quantum wells [3,4]. Besides coupling between levels, two-dimensional spectroscopy can also be used to study various pump-probe induced non-linear phenomena such as incoherent decay of excited states or coherent decay via four-wave mixing signals. The direct generation of multiple harmonics and multiple quantum coherences have been observed at terahertz frequencies in a wide variety of material systems ranging from a two-dimensional electron gas in quantum wells [5,6] to antiferromagnets like $YFeO_3$ [7]. Although a single two-dimensional spectrum does not contain any time information [8], a temporal series of consecutive two-dimensional spectra can be used to obtain information on the dynamics of a system [9,10].

THz time-resolved measurements on QCLs can be used to investigate QCL dynamics, which occur on sub-nanosecond time scales, and the lifetimes of intersubband levels, which are on the order of picoseconds. The dynamics of QCLs are of interest since these lasers can be modulated at high frequencies [11], actively mode-locked at both mid-infrared [12] and terahertz [13,14] frequencies, and used to generate ultra-short pulses [15,16]. As a consequence, pump-probe measurements have been used to obtain information on the gain recovery time and intersubband lifetimes in both mid-infrared [17,18] and THz [19,20] QCLs. Pump-probe measurements have also been used to explore the dynamics of the injector or upper-state lifetimes in mid-infrared QCLs [21]. If the pump and probe beams are coherent, information on the injector and upper state lifetimes can be obtained by taking a two-dimensional scan along two independent time-axis [22], thus allowing the ultrafast coherent transfer of electrons between the injector and upper laser state to be measured in mid-infrared QCLs [21,22].

In this work, we perform coherent collinear two-dimensional THz pump-probe measurements on a THz QCL. A weak THz seed pulse is injected into the laser cavity, which then experiences a large amplification when the QCL is gain switched with a nanosecond bias pulse. After amplification, the seed pulse becomes an effective pump pulse, which is followed by a second THz probe pulse that is injected into the laser cavity. By using gain switching we eliminate the need to directly generate a strong pump field as required in previous works [5–7].

In contrast to conventional pump-probe spectroscopy schemes, the phase between the THz seed pulse and the probe is fixed and the electric field of the probe pulse is measured directly in time via free space electro-optic sampling. This allows us to perform a two-dimensional scan in time, which can then be Fourier-transformed along both dimensions to obtain a 2D spectrum. Furthermore, the dynamics of the peaks in the 2D spectra are explored by examining a series of low-resolution 2D spectra with a temporal spacing of 1 picosecond.

2. Measurement set-up

The investigated sample is a bound-to-continuum THz QCL with an emission frequency at 2.2 THz [23]. The device was indium-bonded on a copper sub-mount electro-plated with gold and operated in an optical cryostat at a temperature of 10 K. The length of the QCL is 3 mm and the width of the ridge is approximately 200 μm.

Optics EXPRESS

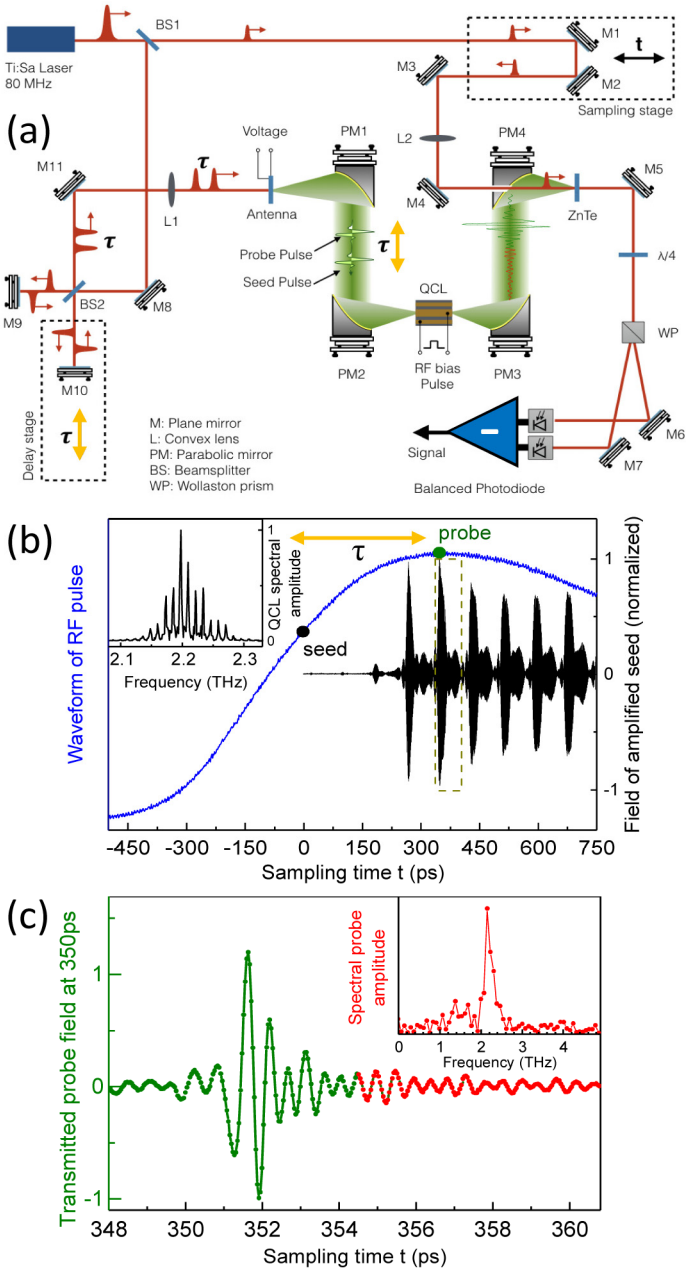

Fig. 1. (a) Two THz pulses are injected into the QCL. A RF bias pulse drives the QCL above threshold and amplifies the first THz pulse (the seed). The second THz pulse (the probe) is injected into the QCL at a later time. (b) The RF bias pulse (blue) and the amplified seed (black). Insert: Fourier transform of the amplified seed. (c) Transmitted probe pulse injected at 350 ps. The probe is modulated for lock-in detection to remove the seed (pump) from signal. Red: Portion of the probe field amplified by the QCL. It is longer than the incident pulse on account of the narrower QCL gain bandwidth. Insert: Fourier transform of the transmitted probe.

The laser was processed as a surface plasmon waveguide [24] that confines a portion of the mode to the active region of the QCL with the aid of a heavily doped n + + layer grown at the bottom of the active region. As shown in Fig. 1(a), two consecutive femtosecond laser

Optics EXPRESS

pulses, produced by a Ti:Sapphire mode-locked laser with a 80 MHz repetition rate, are used to generate two consecutive broadband THz pulses.

Consecutive laser pulses are realized by sending the laser pulse through a Michelson-interferometer with one mirror on a variable delay line. The femtosecond laser pulses are then used to illuminate an interdigitated photoconductive antenna, processed on a low-temperature (LT) grown GaAs substrate [25]. The generation of consecutive THz pulses is made possible due to the sub-picosecond trapping and recombination lifetimes in LT-GaAs [26]. This prevents the screening of the bias field for the second laser pulse by the photo-injected carriers associated with the first laser pulse.

The consecutive THz pulses are then focused into one facet of the QCL cavity using off-axis parabolic mirrors (not shown in Fig. 1(a)). The electric field of the THz pulses transmitted through the opposite facet is then measured via free space electro-optic sampling [27,28]. Immediately after the arrival of the first THz pulse (the seed), the gain of the QCL is driven above its threshold with an RF bias pulse. Figure 1(b) shows the RF pulse (blue curve) that has a sub-nanosecond rise time. These RF bias pulses are generated by illuminating a high-speed photodiode with a portion of the femtosecond laser beam. This ensures that the electrical bias pulses are synchronized to the 80 MHz repetition rate of the femtosecond laser. Before being sent to the QCL, the RF bias pulses are amplified with a broad-band RF power amplifier. The THz seed pulses are amplified by the QCL and undergo multiple round-trips in the QCL cavity [29,30]. In contrast to the steady-state laser operation [31–33], the gain is not equal to the losses during the rise-time of the RF bias pulses. This permits large amplification of the injected THz seed pulse [34].

The amplified THz field transmitted through the opposite face of the QCL is shown as function of time in Fig. 1(b) (black curve). The transmitted field appears as a train of short electric field pulses for multiple integers of the round-trip time (~81 ps for this QCL). Initially, the seed pulse experiences a large amplification, however after ~300 ps the amplified seed pulses are strong enough to saturate the gain and hence amplification ceases.

The second THz pulse (the probe) is then injected into the QCL after a time greater than 345 ps. The amplified seed pulse (black curve; Fig. 1(b)) is removed from the transmitted probe field (Fig. 1(c)) by modulating the THz probe pulse with an optical chopper [35] and detecting the electro-optic signal with a lock-in amplifier. In contrast to references [19,20], we investigate the laser dynamics above the laser threshold. Above threshold, the pump field (i.e. the laser field) is distributed along the entire length of the laser cavity due to multiple reflections. Nevertheless, in the output of the QCL, we observe well-defined pulses that are separated by the round-trip time of the laser cavity.

3. Two-dimensional spectra

There are two time-axes in the measurement: the sampling time – t, which is varied by moving the delay line for the electro-optic detection and the delay time – τ, which is varied by moving the delay line in one arm of the Michelson interferometer. (There needs to be two independent time axes in order to obtain two independent frequencies axes for the 2D spectra.) The delay time represents the delay between the injection of the seed pulse (represented by the black circle in Fig. 1(b)) and the injection of the probe pulse (represented by the green circle in Fig. 1(b)). In Figs. 1(b) and 1(c), we have defined both time-axes such that $\tau = 0$ and $t = 0$ corresponds to the injection of the seed pulse. The spectral amplitudes of the fields in Figs. 1(b) and 1(c) are shown in the corresponding insets. The spectral amplitude of the amplified seed pulse, Fig. 1(b), consists of a series of longitudinal cavity modes centred at 2.2 THz with a spacing of 12.2 GHz. To increase the signal-to-noise ratio and speed up the acquisition time only the portion of the

Optics EXPRESS

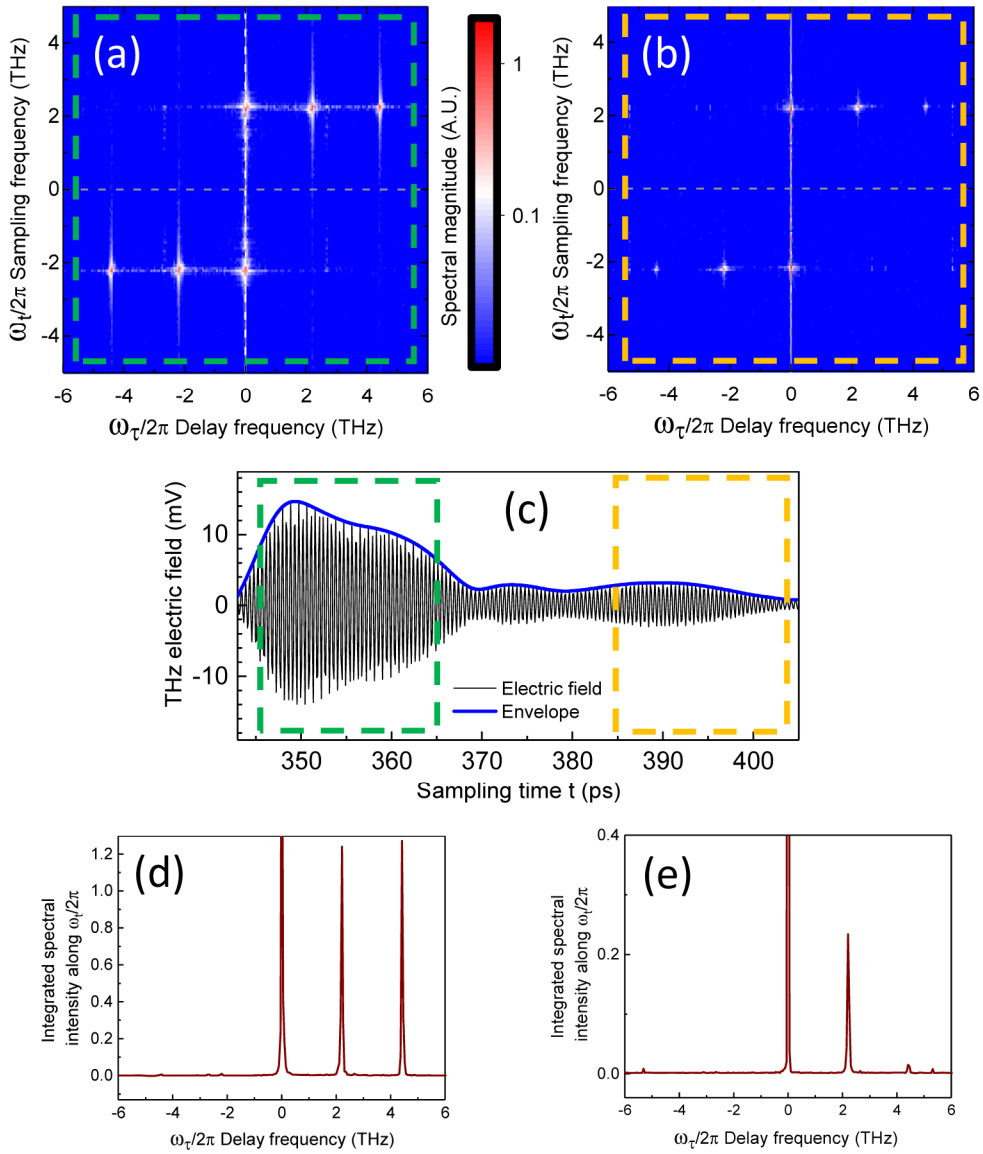

Fig. 2. Two-dimensional spectra of the THz probe for delay times τ = 345-365 ps (a) and τ = 385-405 ps (b). The sampling time window is 13 ps. (c) The amplified seed (the pump) versus time. The dashed rectangles correspond to the delay times in (a) and (b). The square of the spectral amplitude is integrated along the sampling frequency for the upper half of the two-dimensional spectra and shown in (d) and (e) for parts (a) and (b), respectively.

probe field in red, see Fig. 1(c), is recorded, which is representative of the amplification caused by the relatively narrow gain bandwidth of the QCL.

In addition to the frequency information obtained by taking the Fourier transform of the probe with respect to the sampling time, additional information can be obtained by taking another Fourier transform of the probe with respect to the delay time. This results in a 2D spectrum, shown in Figs. 2(a) and 2(b), where the frequency axis obtained from the delay time ω_τ is plotted on the horizontal axis and the frequency axis obtained from probe time ω_t is plotted on the vertical axis. For all two-dimensional spectra the window of sampling time scan is moved along with delay time so that relative position of the sampling time window

Optics EXPRESS

with respect to the probe pulse is fixed. The origin of the frequency axis ($\omega_\tau = 0$, $\omega_t = 0$) corresponds to the centre point of the two-dimensional spectra. Since the fields are real, the 2D Fourier transform is symmetric in the sense that the diagonal quadrants are equal [i.e., if S represent the two-dimensional spectra, $S(\omega_\tau, \omega_t) = S(-\omega_\tau, \omega_t)$] and $S(\omega_\tau, -\omega_t) = S(-\omega_\tau, \omega_t)$. Thus, two of the quadrants shown in Figs. 2(a) and 2(b) are redundant, but are included in Fig. 2 for completeness. The quadrant with two positive frequencies is referred to as the non-rephasing quadrant, while the quadrant with one positive and one negative frequency is referred to as the rephasing quadrant. For conventional two-dimensional spectroscopy, any peaks arising from photon echoes would originate in the rephrasing quadrant. Since the width of the QCL transitions are expected to arise from decoherence times and the multiple levels in the conduction band of the QCL structure [33], we do not expect the QCL transition to be predominantly in-homogeneously broadened. Thus, the two-dimensional peaks are expected to be in the non-rephasing quadrant. In Figs. 2(a) and 2(b), it is seen that the major peaks are indeed in the non-rephasing quadrants of the two-dimensional spectra. Nevertheless, there are several minor peaks in the rephrasing portion of the two dimensional spectra. However, when the integrated spectral intensity is plotted, as shown in Figs. 2(d) and 2(e), the minor peaks at negative frequencies (which correspond to rephasing) are significantly less prominent.

The two-dimensional spectra taken for delay times corresponding to strong (τ = 345-365 ps) and weak (τ = 385-405 ps) field sections of the amplified seed are shown in Figs. 2(a) and 2(b), respectively. For both the strong and weak field sections, there are three main peaks in the two-dimensional spectra along the zero, first, and second harmonics of the delay frequency axis ω_τ, for a sampling frequency equal to the laser frequency ω_0, i.e. at the points $S(\omega_\tau = 0, \omega_t = \omega_0)$, $S(\omega_\tau = \omega_0, \omega_t = \omega_0)$, and $S(\omega_\tau = 2\omega_0, \omega_t = \omega_0)$, respectively.

The peak at $S(\omega_\tau = 0, \omega_t = \omega_0)$ corresponds to the rectified component of the instantaneous intensity of the amplified seed. This peak does not arise from any DC offset in the probe spectra which would produce a peak at the origin $S(\omega_\tau = 0, \omega_t = 0)$. The peak at $S(\omega_\tau = \omega_0, \omega_t = \omega_0)$ corresponds to the probe response to the electric field of the amplified seed and can be viewed as an interference term.

The peak at $S(\omega_\tau = 2\omega_0, \omega_t = \omega_0)$ is the response of the probe to the $2\omega_0$ component of the instantaneous intensity (or square of the amplified seed field). This peak does not represent second harmonic generation which would produce probe photons with frequency $2\omega_0$ and thus correspond to the point at $(\omega_\tau = \omega_0, \omega_t = 2\omega_0)$. Rather, the peak at $S(\omega_\tau = 2\omega_0, \omega_t = \omega_0)$ is analogous to a double quantum coherence found in conventional two-dimensional spectroscopy [36–38]. However, in this work the length of the QCL is not optically thin. As a result the $S(\omega_\tau = 2\omega_0, \omega_t = \omega_0)$ signal could arise from spatial hole burning effects where the gain is modulated across the length of the cavity from the saturation effects that are proportional to the $2\omega_0$ component of the instantaneous intensity. The amplitude of the $S(\omega_\tau = 2\omega_0, \omega_t = \omega_0)$ peak is significantly reduced for the weak field spectra compared to the strong field region (see Fig. 2(c)). This can be seen more clearly in Figs. 2(d) and 2(e), where the two-dimensional spectra are integrated for positive sampling frequencies for the strong and weak sections of the amplified seed field, respectively.

4. Time dependence of the nonlinear peaks

The dependence of the $S(\omega_\tau = 2\omega_0, \omega_t = \omega_0)$ peak on the strength of the amplified seed field (the effective pump field) is explored as a function of sampling time. This is realized by reducing the duration of the time windows used for the two-dimensional spectra to 1ps for both the delay time and sampling time. The amplitudes of the $S(\omega_\tau = 2\omega_0, \omega_t = \omega_0)$ peak are then plotted (dark squares) as a function of time as shown in Fig. 3 along with the square of the amplified seed envelope (blue line). The $S(\omega_\tau = 2\omega_0, \omega_t = \omega_0)$ signal roughly follows the general shape of the square of the field envelope. The origin of the $S(\omega_\tau = 2\omega_0, \omega_t = \omega_0)$ peak could be either due to

Optics EXPRESS

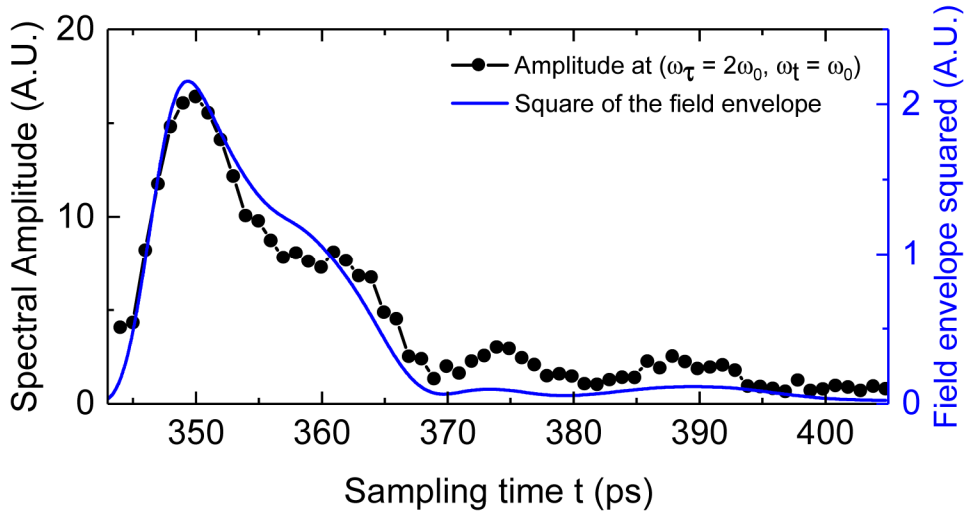

Fig. 3. The black squares show the spectral amplitude of the $S(\omega_\tau = 2\omega_0, \omega_t = \omega_0)$ peak as a function of sampling time t for a series of two-dimensional spectra with a scan duration of approximately 1 ps for both the delay and sampling times. The blue line shows the envelope of the instantaneous intensity as a function of the sampling time.

a modulation of the gain due to saturation, which produces a spatial-hole burning response [39], or due to a non-linear response involving a 3rd virtual level. In the latter case, an electron would be promoted from the lower laser state to a virtual level above the upper laser state with two photons – leading to an oscillation at twice the laser frequency along the delay frequency axis. The electron in the virtual level would then be brought to the upper state via the emission of a single photon – leading to an oscillation at the laser frequency along the sampling time axis. This would essentially be a double quantum coherence. The dependence of the rectified peak $S(\omega_\tau = 0, \omega_t = \omega_0)$ on the strength of the amplified probe as a function of time is also investigated, see Fig. 4, by reducing the duration of the delay and sampling times. In contrast to the $S(\omega_\tau = 2\omega_0, \omega_t = \omega_0)$ peak, the rectified peak at $S(\omega_\tau = 0, \omega_t = \omega_0)$ is found to decrease when the envelope (blue curve) of the amplified probe increases to a maximum value and then recovers when the envelope of the amplified probe decreases. The temporal response of this $S(\omega_\tau = 0, \omega_t = \omega_0)$ peak is reminiscent of a classic pump-probe response where the pump saturate the response of the probe. The rectified response in Figs. 2(a) and 2(b) is also quite broad along the probe frequency (ω_t) axis, which is a typical feature for a pump-probe peak in a 2D spectrum [7].

The $S(\omega_\tau = 0, \omega_t = \omega_0)$ peak recovers after ~10 picoseconds, which is slightly less than previous reports on the gain recovery times in THz QCLs [19,20] measured below threshold. However, the gain recovery in quantum cascade lasers can be quite complicated, as many different levels are involved in this process. For example, the gain recovery may be affected by carrier transport across the mini-bands and electron transfer between the injector and upper laser state. The gradual decrease of the amplitude of the $S(\omega_\tau = 0, \omega_t = \omega_0)$ peak over long time scales (from 380 ps to 405 ps) may be due to the distributed electric field in the cavity. Since we are only detecting the out-coupling field in Fig. 1(b), standing waves (from multiple reflections) inside the cavity might contribute to an internal electric field for times where the out-coupled electric field of the pump, Fig. 1(b), is low. The use of a longer laser cavity could minimize these effects. Additional contributions to the internal electric field might arise from the build up of spontaneous emission, which cannot be detected [40] with electro-optic sampling.

Optics EXPRESS

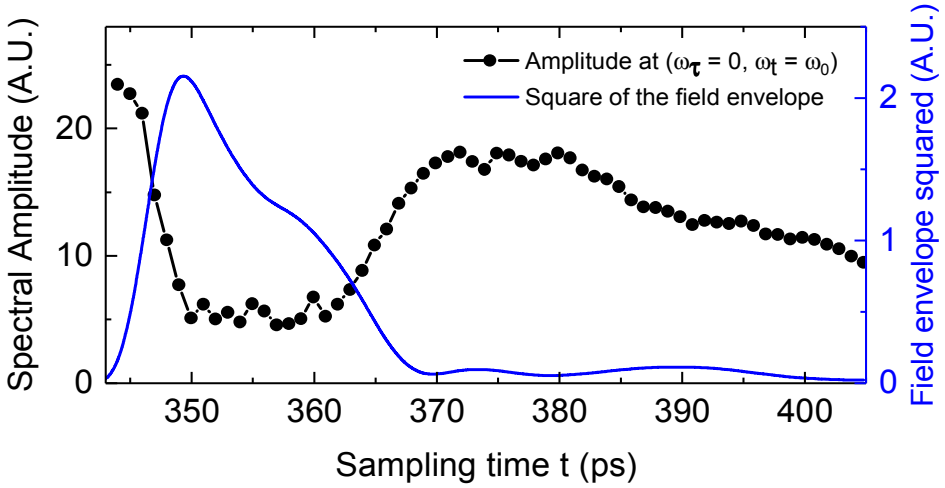

Fig. 4. The black squares show the spectral amplitude of the $S(\omega_\tau = 0, \omega_t = \omega_0)$ peak as a function of the sampling time t for a series of two-dimensional spectra with a scan duration of approximately 1 ps for both the delay and sampling times. The blue line shows the envelope of the instantaneous intensity as a function of sampling time.

5. Conclusion

We have recorded two-dimensional pump-probe spectra of a THz QCL above laser threshold. The two-dimensional spectra were obtained by injecting two broadband THz pulses into a QCL with a variable time delay. Gain switching of the QCL was used to amplify the first THz pulse in order to generate a strong field to saturate the gain. The field of the second THz pulse was then used to measure the response of the strong seed field by varying the delay time with respect to the first THz pulse. The two-dimensional spectra were found to consist of multiple peaks along the delay frequency axis. The peak at zero delay frequency was observed to saturate when the intensity of the amplified seed pulse was maximized, while the peak at the second harmonic of the laser frequency was found to be proportional to the instantaneous intensity. These measurements demonstrate how pump-probe information from THz QCL can be obtained with two-dimensional spectroscopy. By using injection seeding technique, the requirement to generate a strong THz field is removed. This enables an 80 MHz femtosecond oscillator that generate weak THz pulses for non-linear measurements. Further two-dimensional spectroscopic measurements could enable coherent transport, the coherence between the injector and upper laser state in resonant tunnelling for injection of carriers into the upper laser state, the degree of inhomogeneous broadening and further nonlinear effects in QCLs to be explored.

Funding

Bundesministerium für Bildung und Forschung (BMBF) (Q.com-H16KIS0109); Deutsche Forschungsgemeinschaft (DFG) (TRR160); Deutsch-Französische Hochschule (DFH-UFA) (CDFA-05-06); Ministerium für Innovation, Wissenschaft und Forschung (MIWF NRW) (Referat 221); International Max Planck Research School (IMPRS-SurMat); Ruhr Universität Bochum Research School PLUS; Agence nationale de la recherche (ANR) (ANR-12-NANO-0014); Engineering and Physical Sciences Research Council (EP/J017671/1); FET Open - European Commission (ULTRAQCL 665158); Wolfson Foundation; Royal Society.